Michel, G. W., Becker, M., Reigber, C., Tibi, R., Yu, Y. Q., Zhu, S. Y. (2001): Regional GPS data confirm high strain accumulation prior to the 2000 June 4 Mw = 7.8 earthquake at southeast Sumatra. - Geophysical Journal International, 146, 3, pp. 571—582.

DOI: http://doi.org/10.1046/j.0956-540x.2001.01469.x

Geophys. J. Int. (2001) **146,** 571–582

Regional GPS data confirm high strain accumulation prior to the 2000 June 4 $M_w = 7.8$ earthquake at southeast Sumatra

G. W. Michel,[1] M. Becker,[2,*] Ch. Reigber,[1] R. Tibi,[1] Y. Q. Yu[1] and S. Y. Zhu[1]

[1] *GeoForschungsZentrum Potsdam (GFZ), Telegrafenberg,* 14473 *Potsdam, Division* 1 & 2, *Germany. E-mail: fault@gfz-potsdam.de*
[2] *Bundesamt für Kartographie und Geodäsie, Frankfurt am Main, Germany*

Accepted 2001 March 23. Received 2001 January 23; in original form 2000 August 17

SUMMARY

Site velocities derived from repeated measurements in a regional GPS network in Southeast Asia help to constrain the motion of tectonic blocks as well as slip rates along major faults in the area. Using 3-D forward dislocation modelling, the influence of seismic elastic loading and unloading on the measured site motions are approximated. Results suggest that the northwestern Sunda arc is fully coupled seismogenically, whereas its eastern part along Java shows localized deformation. Higher horizontal velocity gradients than expected from the modelling of a fully coupled plate interface west of Manila in the Philippines suggest that deformation may be localized there. Assuming that geodetically derived convergence represents long-term rates, accumulated geodetic moments are compared to those derived using seismic data from 1977 to 2000 (Harvard CMT catalogue). If areas displaying localized deformation are dominated by creep processes, the largest difference between accumulated and seismically released deformation is located where the 2000 June 4 $M_w = 7.8$ Sumatra earthquake occurred.

Key words: earthquakes, geodesy, geodynamics, seismicity.

1 INTRODUCTION

Bounded by subduction zones and hosting the triple plate junction between Sundaland (Wilson *et al.* 1998), the Australian and the Pacific/Philippine Sea plates, Southeast Asia is one of the world's most active tectonic areas. With several earthquakes with magnitudes above 7 occurring every year, high seismicity concentrates on active plate boundaries (Cardwell *et al.* 1980) and/or is distributed over wider transition zones between adjoining plates (Rangin *et al.* 1999). Considering fault domains and taking available geodetic and seismotectonic information into account, cumulative seismic and geodetic moments were compared for the period from 1977 to 2000 ('moment budget'). Whereas instrumental and historical seismicity records indicate that the Sunda arc has been highly affected by large to major earthquakes in the northwestern part, large events have been almost absent along its southeastern extremity (Newcomb & McCann 1987; Pacheco & Sykes 1992). Furthermore, high seismicity and frequent large earthquakes have affected the Philippine arc east of the Philippines, whereas the northwestern subduction zone along the Manila trench appears to be less active seismically (Cardwell *et al.* 1980). This is the opposite of what is expected from plate convergence rates, which increase from west to east along the Sunda arc and are higher along the Manila arc than along the Philippine arc (see below). This paper deals with the results from recently published regional GEODYSSEA GPS measurements (Becker *et al.* 2000) and interpretative modelling. Our aims are to approximate a fault-and-block model for the area and derive long-term slip rates along faults. In order to do this, we model the effects of elastic deformation along the bounding faults of the estimated blocks. Results are then tested against measured site motions taking into consideration the validity of a 'full seismogenic coupling' model in the study area. The method used includes forward dislocation modelling constrained by using the approximate geometries of major active faults and assuming that all faults are fully coupled seismogenically. The model gives a good explanation of site movements that deviate from the 'rigid' block motions along some block-bounding faults. However, it fails to describe site motions along others. Assuming that the detected differences in modelled and measured deformation behaviour reflect the longer-term (several apparent seismic cycles) capability or incapability of certain fault segments to accumulate stresses and strains, discrepancies between released seismic moments and accumulated (geodetic) moments are reconsidered. The maximum resolving accumulated moment is located where a major earthquake occurred in southeast Sumatra on June 4 2000. Source parameters of this earthquake were investigated using teleseismic data from broadband stations. Fault plane solutions for the best-fitting model indicate thrust and strike-slip faulting with a complex rupture mechanism.

* Now at: Institut für Geodäsie, Universität der Bundeswehr, 85577 Neubiberg, Germany.

2 DATA SOURCE AND FAULT-AND-BLOCK MODEL

Data sources used in this study include seismotectonic information from the literature (see below), teleseismic records (Harvard CMT solutions; Dziewonski *et al.* 1981), information from global plate motion models (NUVEL1A; DeMets *et al.* 1990, 1994) and regional geodetic measurements (Wilson *et al.* 1998; Becker *et al.* 2000; Michel *et al.* 2000). The crucial part of the geodetic data comes from repeated measurements performed under the GEODYSSEA (geodynamics of S and SE Asia) project, which was aimed at studying plate motions and long-term crustal deformation within a GPS network (Fig. 1) covering a 4000 km by 4000 km area in Southeast Asia (Wilson *et al.* 1998). Measurements were made in 1994, 1996 and 1998. Results have filled an important 'geodetic' gap between the Indian, Australian and Philippine Sea plates and helped to constrain the motion of Sundaland (Fig. 2). Sundaland was previously suggested to be either a southeastern extremity of Eurasia (DeMets *et al.* 1990, 1994; Tregoning *et al.* 1994) or continuously deforming (Kreemer *et al.* 2000) or an assemblage of blocks extruding east to southeast as a consequence of the ongoing penetration of India into Eurasia (Peltzer & Saucier 1996 and references therein). Earlier geodetic results obtained from across the area suffered from a poorly defined global reference system and fewer data (Simons *et al.* 1999; Chamot-Rooke & Le Pichon 1999), besides offering restricted areal coverage (Puntodewo *et al.* 1994; Yu *et al.* 1999) and concentrating on seismically active boundaries (Puntodewo *et al.* 1994; Genrich *et al.* 1996).

The GEODYSSEA data sets were used to approximate a kinematic fault-and-block model. Teleseismic data from crustal earthquakes taken from January 1977 to June 1999 (Harvard CMT solutions) and data from the literature describing the traces of faults and the distribution of fault segments (Tjia 1978; Hamilton 1979; Newcomb & McCann 1987; Gudmundsson *et al.* 1998) were used to map active faults, estimate their traces and approximate slip directions, slip partitioning conditions (McCaffrey 1996) and seismic slip rates. Rectangular 2-D fault planes were ascribed to those seismic domains that were assumed to represent major faults. Assuming that the fault segments under study are capable of producing earthquakes of $M = 8$ or above, scaling laws were taken into account (Scholz 1982; Scholz & Aviles 1986; Wells & Coppersmith 1994). The lower edge of the seismogenic interface (and elastic loading; see Section 3) was approximated by the average depth of the earthquake hypocentres (< 50 km depth) plus their 1σ errors. Fault planes were chosen in accordance with the seismotectonic situation and fault dips from the composite fault plane solutions served as the average dip of the fault segments considered (Table 1). The

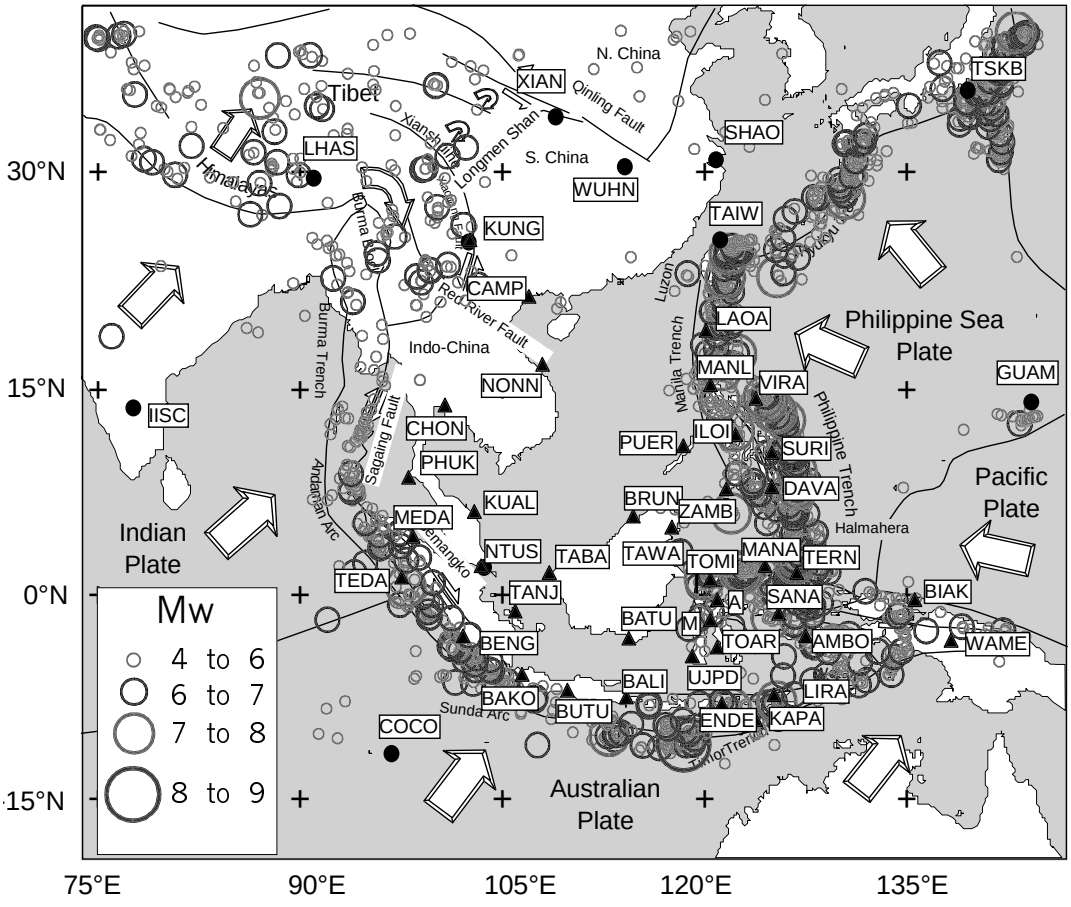

Figure 1. Crustal earthquakes (1977–2000, CMT Harvard catalogue, depth < 50 km) and geodetic stations. Small labelled dots represent permanent stations from the IGS and triangles represent the GEODYSSEA GPS observation stations. Large arrows show directions of plate motions (ITRF97). Circles represent epicentres of crustal earthquakes. Black solid curves depict approximate trends of major active faults. The central part of the figure displays a block almost free of earthquakes. This block was defined as 'rigid' and moving at a rate of between 10 and 13 mm yr^{-1} roughly east with respect to 'stable' Eurasia (Becker *et al.* 2000; Michel *et al.* 2000).

Table 1. Fault segments and comparison of geodetic and earthquake moments (1977 to June 1999).

Name	Long. (°)	Lat. (°)	Slip (mm yr^{-1})	Length (km)	Dip (°)	Width (km)	M0Eq (N m yr^{-1})	M0GPS-M0Eq (N m yr^{-1})	M0seis/M0GPS
Sumatra/Java									
SUS3	103.59	−4.88	/31	235	89	31	2.5E+018	4.2E+018	0.37
SUS2	99.3	1.62	/33	235	89	18	3.4E+017	3.8E+018	0.08
SUS1	97.69	3.81	/33	392	89	33	7.4E+017	1.2E+019	0.06
SU2T	101.92	−5.05	52/−12	706	17	103	4.8E+018	1.1E+020	0.04
SU1T	97.58	0.17	38/−8	472	16	102	2.9E+018	5.3E+019	0.05
JA1W	107.85	−8.69	72	558	22	99	7.8E+017	1.2E+020	0.01
JA1E	113.59	−10.87	68/−13	670	10	109	2.2E+019	1.3E+020	0.14
ANDS	95.04	4.75	30/−15	707	36	56	5.5E+017	3.9E+019	0.01
ANDN	93.32	12.6	7/−4	792	53	16	7.1E+016	3.0E+018	0.02
ANSS	94.51	7.12	/−27	707	89	31	7.5E+017	1.7E+019	0.04
ANSN	95.33	13.28	−18/−43	792	89	31	5.6E+016	3.5E+019	0.00
The Philippines									
PHIN	125.06	13.55	22/15	352	20	55	1.9E+019	−3.7E+018	1.24
PHIS	126.96	9.36	37/20	500	27	56	1.9E+019	1.6E+019	0.55
MANS	119.53	15.64	57/10	321	29	73	2.8E+017	4.0E+019	0.01
LUZO	123.25	16.45	33/	215	25	66	4.7E+018	9.4E+018	0.33
INFA	120.85	16.00	/25	235	89	28	1.9E+019	−1.4E+019	3.76
MIND	120.89	12.45	/21	461	89	29	2.4E+017	8.3E+018	0.03
VEPA	121.52	13.18	/25	562	89	32	2.2E+017	1.3E+019	0.02
TAIW	120.80	23.09	55/5$_{x)}$	666	50	31	3.3E+019	1.2E+018	0.96
MANN	120.37	19.00	84/	516	28	65	2.0E+018	8.2E+019	0.02
NEGS	121.89	9.36	16/13	278	17	56	1.9E+017	9.6E+018	0.02
COTO	124.51	6.09	27/17	280	38	53	8.9E+016	1.4E+019	0.01
PHFS	125.58	9.00	/16	280	89	37	6.3E+016	5.3E+018	0.01
COTS	124.69	6.84	/19	522	89	40	6.2E+016	1.2E+019	0.01
MOLA	125.96	5.91	25/9	247	26	79	3.5E+018	1.2E+019	0.22
PHSN	123.25	12.84	/15$_{x)}$	630	89	30	0.0E+000	8.6E+018	–
Banda Sea/Moluccas									
MOSE	126.62	1.48	66/	354	21	89	2.8E+019	3.4E+019	0.45
MOSW	125.75	1.86	37/	354	28	68	7.2E+015	2.7E+019	0.00
MINE	122.55	1.86	26/	333	28	60	3.0E+019	−1.4E+019	1.90
MINW	119.72	1.22	37/	225	12	149	3.8E+019	−7.8E+017	1.02
SOSW	125.26	−2.18	/40	477	89	25	2.1E+019	−7.2E+018	1.50
SO2T	133.51	−0.04	46/	472	24	54	7.7E+016	3.5E+019	0.00
JAB1	115.79	−7.74	5/	331	16	73	1.3E+018	2.5E+019	0.34
JAT2	116.89	−10.89	61/	223	30	20	4.0E+016	8.1E+018	0.00
BANT	118.74	−11.27	52/	223	30	151	1.6E+020	−1.1E+020	3.09
JAB2	118.49	−7.99	8/	333	22	69	6.9E+016	5.5E+018	0.01
BAB1	121.69	−7.99	19/	440	35	52	3.1E+019	−1.8E+019	2.31
BAB2	124.95	−7.86	13/	334	35	54	3.8E+019	−3.1E+019	5.54
BATE	129.08	−7.99	11/	385	23	84	9.8E+016	1.1E+019	0.01
BAB3	127.85	−6.73	18/	354	45	44	2.4E+019	−1.6E+019	2.82
BIAK	138.25	−1.55	46/	397	10	144	1.1E+020	−3.1E+019	1.39
BAT1	121.45	−11.88	39/	426	25	71	0.0E+000	3.5E+019	0.00
BAT2	125.75	−10.24	21/	578	25	71	0.0E+000	2.6E+019	0.00

Name: the fault segment characterization as depicted in Fig. 3; Long. and Lat.: the central part of the (virtual) surface outcrop location of planar faults (Fig. 6) (estimated errors depend largely on the available information from literature and may range between 0.2° and 0.5°); Slip: yearly rates of differential motion with first number representing fault-normal component (+: thrust faulting) and second number representing strike-slip component (−for dextral strike-slip faulting, estimated errors 1–6 mm yr^{-1}); Length: length of fault segment (for a discussion on the relative error see text); Dip: fault dip; Width: segment width; M0Eq: earthquake moment rate; M0GPS-M0Eq: difference between geodetic and earthquake moment rates; M0seis/M0GPS: ratio between both moments. ($_{x)}$: half the rate due to reported creep).

upper edge of seismogenic coupling (see modelling section) was set at 10 km for most of the fault segments (Table 1). Upper edges that reach the surface were only considered where wrench faulting near GPS sites indicated high elastic loading/unloading effects. Cumulative seismic slip directions were applied to describe the kinematic characteristics of the fault segments. The threshold distance for ascribing earthquakes to fault segments was set at 60 km. 95 per cent of the earthquake data were ascribed to discrete 2-D fault segments using this criterion. 5 per cent of the earthquakes were attributed to distributed deformation. Moment tensors of events were added and principal strain axes and/or average slip rates along segments were inverted using

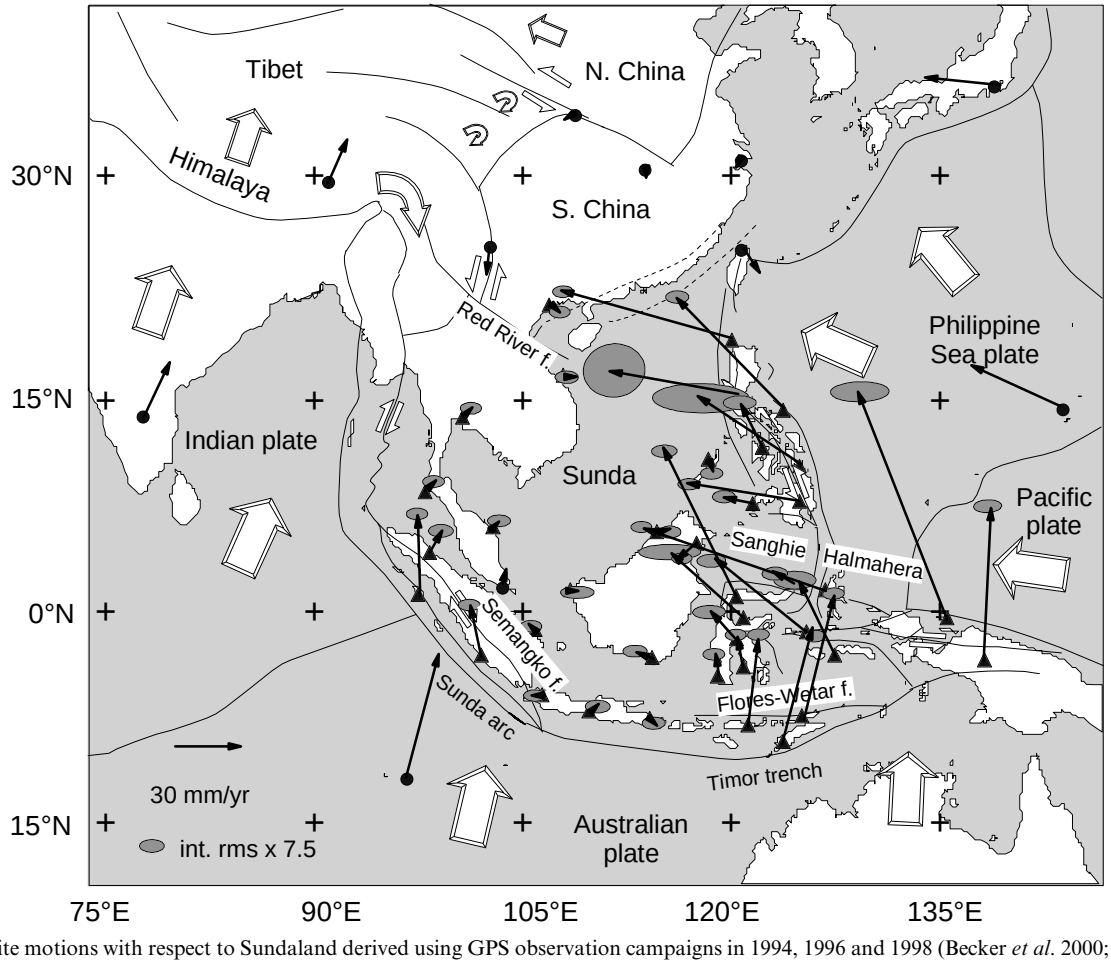

Figure 2. Site motions with respect to Sundaland derived using GPS observation campaigns in 1994, 1996 and 1998 (Becker *et al.* 2000; Michel *et al.* 2000). Error ellipses of the GEODYSSEA solution (see Becker *et al.* 2000) are multiplied by a factor of 7.5 in order to approximate the external error.

Kostrov's (1974) formulation. The rigidity was set at 30 GPa. Table 1 gives the segment dimensions and composite seismic moment rates derived using the studied earthquake information.

Relative NUVEL1A and/or GEODYSSEA motions of adjoining blocks or plates were considered and convergence directions and rates were derived along the different boundaries studied. Oblique convergence directions and rates were partitioned using geometric relationships defined by the characteristics of adjacent faults as described by the cumulative seismic slip directions (McCaffrey 1996 and references therein). Motion of the Sundaland block (Wilson *et al.* 1998; Simons *et al.* 1999) was characterized using site motions on the apparently stable core of this block (Becker *et al.* 2000). The residuals of the site motions of this block are small (Becker *et al.* 2000) (of the order of the internal precision of the solution) after comparison with a best-fitting (solid) block model, suggesting that it is 'rigid' (Simons *et al.* 1999; Chamot-Rooke & LePichon 1999; Michel *et al.* 2000). In order to include the kinematic behaviour of the Australian, Indian, Philippine Sea and Pacific plates in the solution, NUVEL1A Euler poles were applied and relative site motions derived. The computed site motions along plate margins were then compared with the measured site motions. Residuals were attributed to the predicted elastic deformation (see below).

In order to approximate a 'moment budget', that is, to approximate the total implied moment by comparing geodetic moments with cumulative seismic moments for the time span studied, we considered differential site motions along the fault segments defined above using the geodetic results. Taking into account the uncertainties in the teleseismic solutions and segment geometries, errors in cumulative earthquake moments are assumed to reach the same order of magnitude as the derived moments. In order to account for uncertainties in the fault dimensions, results were cross-checked using a model that includes fault segments with uniform lengths.

3 MODELLING OF TRANSIENT ELASTIC LOADING AND RELEASE EFFECTS ON THE SITE MOTIONS

3-D uniform-slip forward dislocation modelling (Okada 1985; Savage 1983) was used to estimate the influence of large to major earthquakes that occurred between campaigns on the GEODYSSEA site motions. This was done using teleseismic information provided by the Harvard CMT catalogue (Dziewonski *et al.* 1981) and scaling laws (Scholz 1982; Scholz & Aviles 1986; Wells & Coppersmith 1994). A similar modelling approach was used to estimate interseismic loading along faults (referred to elsewhere as back-slip approaches). In order to do this we assumed that the measured deformation equals the long-term block (geological) motion minus the coseismic deformation, that is, that interseismic elastic loading is equivalent to the coseismic deformation release with opposite sign (Savage 1983). The purpose was to test whether elastic loading effects along the bounding faults of the major blocks would be large

enough to be estimated from the measurements (see e.g. Freymueller *et al.* 1999). In doing this we considered the effects of seismogenic loading on apparent 'long-term' (geological) site motions and checked if the geodetic model may suffice to approximate changes in loading behaviour along the lines of the major plate boundaries in the study area. Due to the loosely defined rheological parameters of the lower crust and upper mantle, no attempt was made at this stage to try to correct site motions using the viscoelastic behaviour of the lower crust and upper mantle (e.g. Pollitz & Dixon 1998).

Except for the northern part of the Philippine Fault (Duquesnoy *et al.* 1994) and the roughly N–S-trending plate boundary in Taiwan (Yu & Liu 1989), all fault blocks were modelled as fully seismically coupled units (Table 1). Errors involved in the dislocation modelling originate from uncertainties in the rigidity considered, the teleseismic information and the fault geometries and dimensions used. The major error source lies in the locations of the fault segments, the segment dimensions and the earthquake hypocentre determination. Test-runs with end-member boundary conditions (shift of segments and earthquake locations by up to 60 km) revealed uncertainties occasionally higher than 50 per cent for the transient effects being studied. Errors in the estimated slip directions are considered to be of the order of the uncertainties of the geodetic measurements, i.e. approximately 10 per cent.

In order to compare the accommodation of deformation inferred from the historical earthquakes and geodetic data to the southeast of Sumatra with the rupture characteristics of the 2000 June 4 earthquake and to infer the source parameters of this event using teleseismic data recorded by the global seismograph network, we employed the method of Nábelek (1984). The method applies waveform modelling of teleseismic *P* and *SH* waves to invert for source model parameters in a least-squares technique. Teleseismic *P* and *SH* seismograms were deconvolved to ground displacement and high-pass filtered at 0.01 Hz. In computing theoretical seismograms we used the IASP91 (Kennet & Engdahl 1991) velocity model with five layers above 171 km on the source side and a half-space model for the receiver structure. The far-field source time function was parametrized by applying a series of triangular-shaped pulses of 3 s length.

4 RESULTS

Table 1 includes cumulative seismic moments of the 22 yr period under study and accumulated geodetic moment magnitudes derived by extrapolating 4 yr of geodetic results (Becker *et al.* 2000) to the same time span. Stress/strain transfer during and/or after earthquakes (e.g. Stein *et al.* 1997) was neglected for this regional study and strain accumulation and release was treated discretely for the different fault segments studied in this part of the investigations. Fig. 1 shows the distribution of crustal earthquakes in the study area. These earthquakes concentrate on the plate boundaries of Sundaland with the Pacific/Philippine Sea, Australian, Indian and Eurasian plates (Fig. 2; Wilson *et al.* 1998; Chamot-Rooke & LePichon 1999;

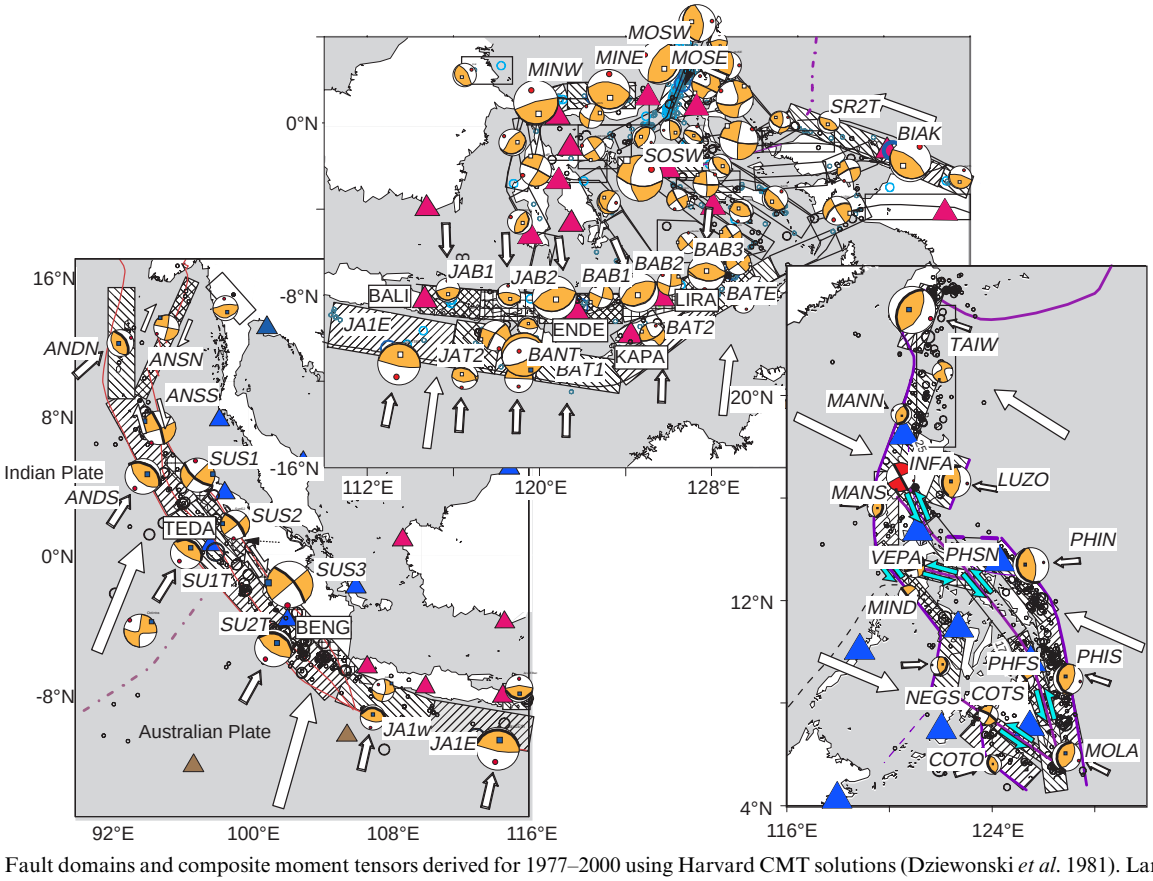

Figure 3. Fault domains and composite moment tensors derived for 1977–2000 using Harvard CMT solutions (Dziewonski *et al.* 1981). Large arrows denote plate convergence directions with respect to Sundaland. Small arrows depict slip directions along fault segments derived using the composite seismic moment tensors at each fault domain (beachballs). Triangles reflect GEODYSSEA GPS stations. Fault segment characterizations coincide with those depicted in Table 1. See text for further discussion.

Simons *et al.* 1999; Michel *et al.* 2000). The Sundaland block was found to be 'rigid' with respect to the precision of the geodetic data taken at the core stations of this block (Michel *et al.* 2000; Fig. 2). Fig. 3 depicts fault segments and composite fault plane solutions derived using data of the Harvard CMT catalogue and information from the literature (see above). Large arrows in the figure denote the directions of relative plate motions; small arrows represent directions of differential site motions along fault segments derived using composite seismic slip directions. Corresponding numbers are included in Table 1. Focal mechanism solutions denote composite solutions of the underlying fault segments (dashed areas). The relative sizes of the focal solutions indicate relative rates of seismic moments. Site motions were fully partitioned according to the available geodetic and seismic information for the two areas in the lower part of Fig. 3, which represent the areas of Sumatra/Java and the Philippines. Seismicity and deformation of the area in the upper part of Fig. 3, which includes the Banda arc and the area of the plate triple junction, are considered to be too complicated to be approximated by a consistent block model using the sparse site motions available. Therefore, we considered differential motions for some major bounding fault segments, relevant for approximating a regional model.

Vectors in Fig. 4 represent the modelled coseismic site motions (1994–1998). Dotted lines connect focal mechanisms with the approximate epicentre locations of large earthquakes indicated in the Harvard CMT catalogue (Dziewonski *et al.* 1981). Coseismic motions were treated separately for the different time spans measured (1994–1996, 1996–1998) and focal mechanisms related to the individual time spans are marked with different colour intensities in Fig. 4. Table 2 shows the relevant numbers of modelled site motions related to the coseismic strain release. Resolving deformations are restricted to the perimeters of the study area, whereas the central part of the area, which represents the core of the Sundaland block, is apparently unaffected by coseismic deformation. As opposed to sites in the Philippines or Irian Jaya and Sulawesi, sites in Sumatra and Java, as well as within the Moluccas and/or Luzon, appear to be unaffected or only slightly affected by coseismic strain release during the 1994–1998 period.

Table 2 and Fig. 5 show the resulting rates of interseismic elastic loading. Numbers are computed taking into account fully seismogenically locked faults. Due to the small distance of certain stations from the plate and block margins, the apparent effects on the site motions are significant along most of the margins studied. Results suggest high loading effects along the entire Sunda arc. In the Philippines, the largest influence of elastic loading is estimated for site LAOA in Luzon, where Sundaland–Philippine Sea plate convergence is considered to be accommodated mainly along the adjacent Manila trench (Yu *et al.* 1999). Large loading effects are also suggested for sites MANA and TERN (Fig. 5), for example, located adjacent to the Sanghie and Halmahera megathrusts (Hamilton 1979), respectively.

Table 2. Computed coseismic and interseismic deformation (mm).

Station	Co 9496		Co 9698		Interseismic		Composite	
	Ve	Vn	Ve	Vn	Ve	Vn	Ve	Vn
ampa	− 18.1	19.9	−0.3	2.9	2.0	−3.6	−7.2	7.8
BAKO	n.d.	n.d.	n.d.	n.d.	1.0	8.4	1.0	8.4
BALI	n.d.	n.d.	n.d.	n.d.	1.0	5.6	1.0	5.6
BENG	n.d.	n.d.	n.d.	n.d.	8.2	5.8	8.2	5.8
BIAK	217.1	886.5	n.d.	n.d.	n.d.	n.d.	108.5	443.3
BUTU	n.d.	n.d.	n.d.	n.d.	2.3	10.7	2.3	10.7
DAVA	n.d.	n.d.	n.d.	n.d.	−1.2	3.3	−1.2	3.3
ILOI	5.3	2.2	n.d.	n.d.	n.d.	n.d.	2.7	1.1
KAPA	1.3	1.7	n.d.	n.d.	−2.1	3.1	−1.5	4.0
LAOA	n.d.	n.d.	n.d.	n.d.	17.0	−6.9	17.0	−6.9
LIRA	−13.5	−3.6	n.d.	n.d.	n.d.	n.d.	−6.7	−1.8
MALI	−2.0	5.4	n.d.	n.d.	n.d.	n.d.	−1.0	2.7
MANA	n.d.	n.d.	n.d.	n.d.	−9.7	4.4	−9.7	4.4
MANL	n.d.	n.d.	n.d.	n.d.	8.8	−2.4	8.8	−2.4
MEDA	n.d.	n.d.	n.d.	n.d.	0.7	2.4	0.7	2.4
SAMP	n.d.	n.d.	n.d.	n.d.	0.7	2.3	0.7	2.3
SANA	n.d.	n.d.	n.d.	n.d.	11.1	0.9	11.1	0.9
SURI	1.5	2.2	4.7	−0.9	−4.4	−1.0	−1.3	−0.3
TAWA	1.7	−1.2	n.d.	n.d.	n.d.	n.d.	0.9	−0.6
TEDA	n.d.	n.d.	n.d.	n.d.	8.3	8.6	8.3	8.6
TERN	n.d.	n.d.	n.d.	n.d.	19.4	−5.9	19.4	−5.9
TOMI	−405.2	36.6	−23.1	31.3	4.0	−18.0	−210.2	15.9
VIRA	n.d.	n.d.	n.d.	n.d.	−5.5	2.2	−5.5	2.2
WAME	−3.2	12.5	n.d.	n.d.	−0.2	−4.6	−1.8	1.7
ZAMB	n.d.	n.d.	n.d.	n.d.	−2.3	1.1	−2.3	1.1

Numbers denote computed amounts of elastic deformation in millimetres above a threshold of 2 mm yr^{-1}. Co9496 represents coseismic strain released during earthquakes above 2.5×10^{-18} N m (Harvard Catalogue) between the 1994 and 1996 campaigns (Co9698 between the 1996 and 1998 campaigns) in the longitudinal (Ve) and latitudinal (Vn) directions. Interseismic means computed yearly rates of horizontal deformation assuming full seismogenic coupling along the studied faults. Composite represents the yearly sum of rates. n.d. indicates that values were not derived.

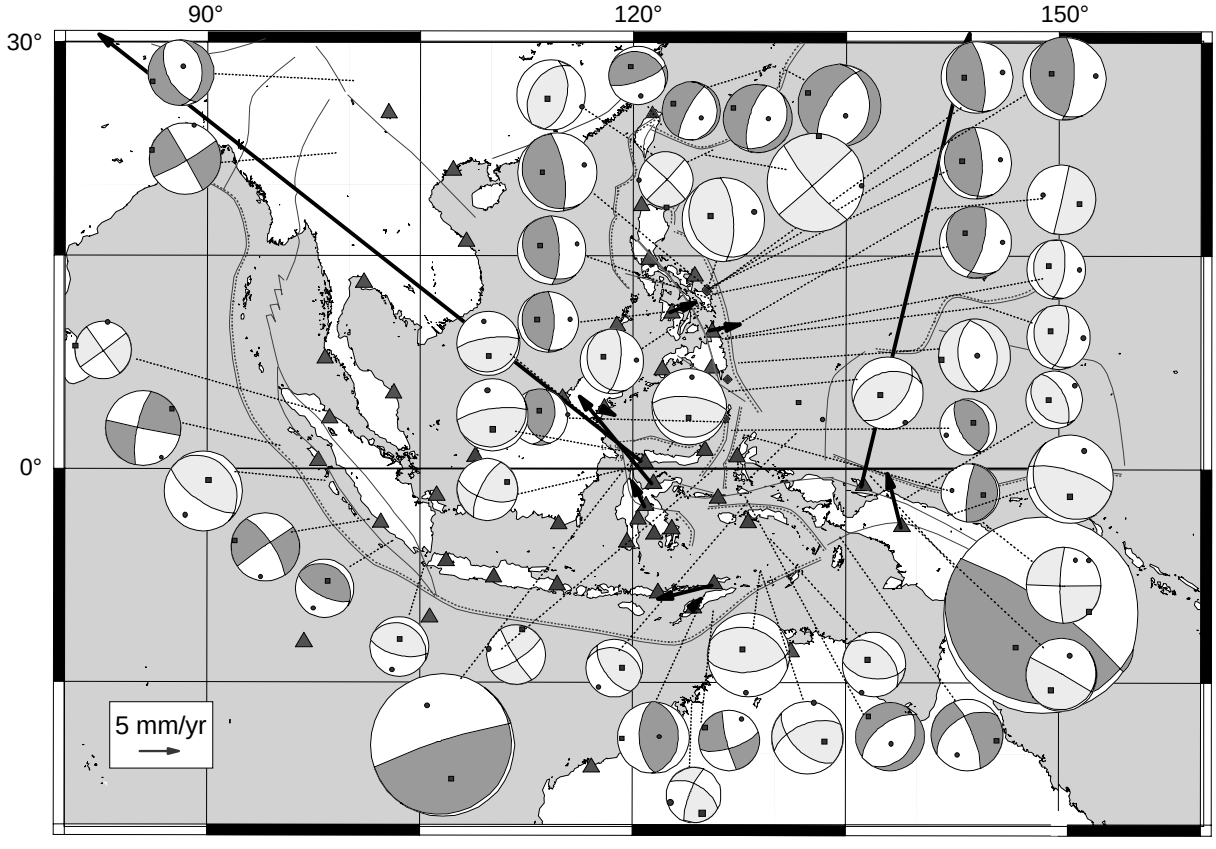

Figure 4. Focal mechanisms (Harvard CMT catalogue; Dziewonski *et al.* 1981) of those large earthquakes with moments equal to or larger than 2.5×10^{18} N m that occurred between campaigns (dark grey: earthquakes between the 1994 and 1996 campaigns; light grey: earthquakes between the 1996 and 1998 campaigns). Relative sizes of the beachballs denote relative sizes of earthquakes. Epicentre locations are displayed by the tip of the dotted lines. Vectors indicate the modelled coseismic deformation at the GPS sites (Table 2).

Taking into account that the Sundaland block is internally stable, residual site motions along its boundaries with respect to a best-fitting 'rigid' block model were assumed to represent the elastic deformation. After subtracting that part of the motion that is parallel to the Semangko (Great Sumatran) fault (TEDA: 26 mm yr^{-1}; BENG: 20 mm yr^{-1}) and taking into account elastic loading along the faults in this area, residuals to the Sundaland block are further reduced by 12 mm yr^{-1} (TEDA) and 11 mm yr^{-1} (BENG), and are now 8 and 2 mm yr^{-1}, respectively. This indicates that residuals are to a large extent compensated when considering full seismogenic coupling along the subduction interface and the Semangko fault (Prawirodirdjo *et al.* 1997).

As opposed to the site motions on Sumatra, site motions in Java appear not to be affected by elastic deformation, and residuals to the 'stable' Sundaland block model are almost negligible (BAKO, BALI, BUTU: 3, 1, 3 ± 3 mm yr^{-1}, respectively; Fig. 3; see for comparison Tregoning *et al.* 1994). Vectors in Fig. 6 demonstrate these results. Red vectors depict the residual site motions of the elastic loading model with respect to Sundaland. Related velocities exceed velocities computed in the model that excludes seismic loading (green vectors) by a considerable margin. This suggests that deformation appears to be highly localized along the plate interface and/or along any other fault south of the measured sites in Java. We conclude that the Java margin may not or may only slightly be affected by interseismic elastic loading.

Full coupling along the Sanghie and Halmahera megathrusts reduces residual site motions of MANA and TERN (to the relevant block models of Sundaland and the Philippine Sea plate) by 9 and 6 mm yr^{-1} and 7 mm yr^{-1}, respectively. In contrast to the eastward-vergent Philippine subduction zone, which shows high ratios of seismic versus geodetic slip rates (see below), the western bounding faults (Manila–Negros trench) of the Philippines show very low ratios. This indicates that, unlike what is indicated in the historical record before 1977 (Pacheco & Sykes 1992), large or major earthquakes have not struck the western bounding fault zones of the Philippines since 1977. Modelled elastic loading along the Manila trench even increases the difference between site motions predicted by the approximated fault-and-block model and measured site motions of the site LOAO (23 ± 4 mm yr^{-1}) by 7 mm yr^{-1}.

A fully seismically coupled S-verging plate interface along the Timor trench would account for only a fraction of the measured motion of ENDE, KAPA and LIRA, with residuals of 35, 52, 55 ± 4 mm yr^{-1} remaining. Considering the high seismicity of the back-arc thrust system, this confirms that most of the motion is taken up there, as suggested by Genrich *et al.* (1996) and references therein. Sites CAMP and NONN north and south of the Red River fault system are too far away from the apparently active fault strand to be affected by elastic loading. Differential motion of less than 5 mm yr^{-1} along this part of the fault system is therefore considered to be insignificant (Michel *et al.* 2000; see also Chen *et al.* 2000 for a discussion).

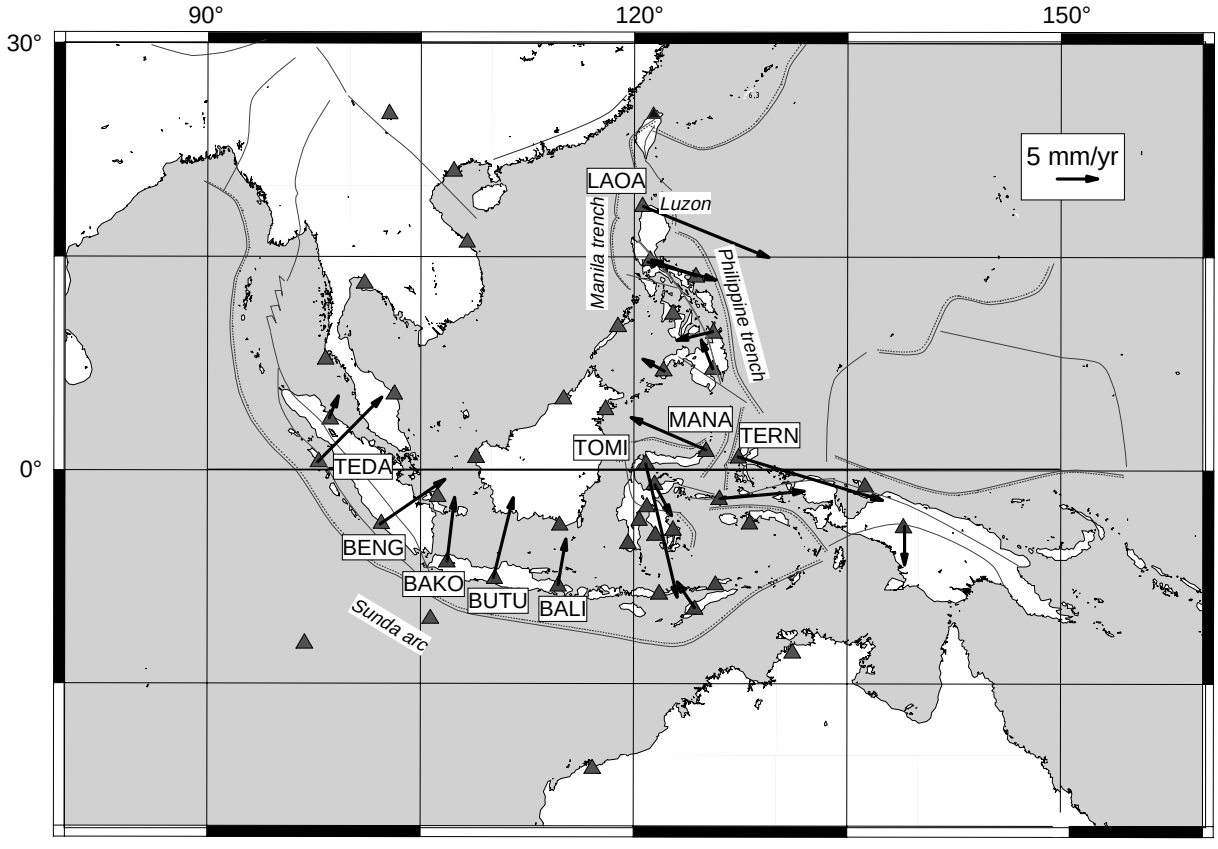

Figure 5. Interseismic elastic deformation from 3-D forward dislocation modelling and dimensions as discussed in the text. In order to derive the elastic deformation at the GPS stations (vectors), full seismogenic coupling was assumed along the faults (Fig. 6) considered.

Fig. 7 shows a 'moment budget', that is, a compilation of the geodetically versus seismically derived deformation over the 22 years studied. The colour distribution in Fig. 7 was derived without taking into account differences in seismogenic coupling as considered above. Red colours represent a surplus in geodetic deformation; blue colours indicate an excess in seismic deformation. Assuming that the geodetic deformation represents the tectonic loading in the brittle part of the crust, this figure suggests that the greatest accumulated deformations that have not been accommodated by seismic faulting during the studied time span are located along the Java trench, along the Manila trench, in the region of Halmahera, along the western New Guinea trench and at southeast Sumatra. The 'moment budget' in the upper right of Fig. 7 was computed assuming that the fault segments studied show equal (averaged) lengths. Conservation of the overall moment was invoked and an average resolving length of 510 km was obtained for each segment. Results of this approach essentially corroborate results of the more complex procedure that involves individually defined seismotectonic domains and fault lengths (see Table 1).

Considering that apparent localized deformation along the Java margin and Manila trench is not in favour of seismically coupled plate interfaces, the largest ratio of accumulated geodetic to seismic deformation is located southeast of Sumatra, where the devastating major earthquake ($M_w = 7.8$) occurred on June 4 2000. The centroid solution derived for this earthquake indicates that rupture occurred at about 40 km depth. The centroid mechanism derived herein shows a thrust faulting mechanism, suggestive of a rupture process on the seismogenic portion of the interface between the Australian plate (and/or transition between the Indian and Australian plates; Gordon *et al*. 1990, 1998) and Sundaland. A seismic moment of 7.3×10^{20} N m was inferred, which corresponds to a moment magnitude (M_w) of 7.8. Rupture lasted about 55 s. The best source model comprises three subevents that differ significantly in their focal mechanisms (Table 3, Fig. 8), suggesting that rupture occurred along a curved fault plane, or on several planes of different orientation. The estimated values for the average dislocation vary between about 2 and 4 m.

Table 3. Source parameters of the 2000 June 4 Sumatra earthquake.

	Strike (°)	Dip (°)	Rake (°)	M_0 (N m)	Length (km)	SD (MPa)	AS (m)
NP1	99	54	114	7.3×10^{20}			
NP2	242	42	61				
S1a	192	60	33	1.7×10^{20}	40	9	2.1
S1b	84	62	145				
S2a	238	48	72	2.9×10^{20}	40	16	3.6
S2b	84	48	109				
S3	270	22	64	3×10^{20}	50	13	3.0

NP1 and NP2: nodal planes of the centroid solution; S1/S2a, b, S3: focal mechanisms of the three rupture episodes (S3 approximates the interface between the Australian and Sundaland plates); M_0: derived seismic moment. The Length of the rupture plane has been computed from using the best-fitting rupture velocity of 2 km s^{-1}. Static stress drop (SD) and average slip (AS) were derived assuming a uniform width of 30 km for the ruptured portion of the seismogenic zone and a rigidity of 66 GPa.

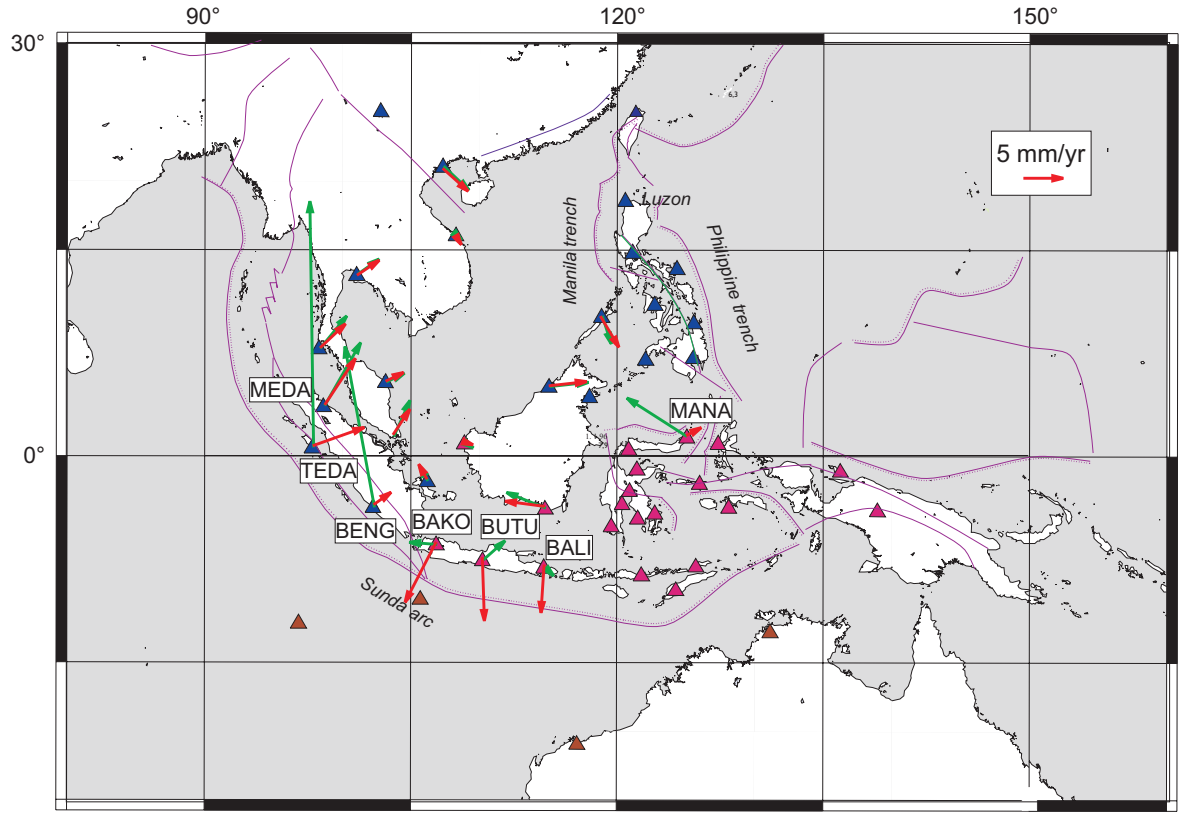

Figure 6. Measured minus modelled Sundaland site motions. Green vectors denote site motions with respect to Sundaland, which were derived directly from the GEODYSSEA measurements. Red vectors indicate site motions with respect to Sundaland that were corrected assuming elastic loading along the bounding faults of the Sundaland block as well as pure strike-slip faulting of between 20 and 30 mm yr^{-1} along the Semangko fault (see text). As opposed to site MANA or sites along the southwestern boundary of the block, which show small residuals to the 'rigid' block motion after correction, sites in Java show significantly larger residuals if elastic loading is taken into account.

5 DISCUSSION

Space geodetic measurements of the 4000 km by 4000 km GEODYSSEA network along with global plate motion models helped us to derive a kinematic block model for Southeast Asia. Using additional information from the literature and seismotectonics of the area, slip rates for major active intraplate and interplate faults were constrained. Dislocation modelling was used to test whether elastic loading and release effects might be detectable in the regional GEODYSSEA site motions. Results suggest that major earthquakes that occurred between measurements had a profound effect on some of the geodetic results. In addition, elastic loading may well be seen as deviations in site motions from the 'rigid' block models where plate boundaries adjacent to measured sites show full seismogenic coupling. This is especially true for the Sundaland block, which shows very low internal strains ($<2\times10^{-8}$ yr^{-1}; Michel *et al.* 2000) and is well constrained by the data used. Testing these results with the measured data suggests that the loading behaviour changes along the Sunda arc. According to our results, highly distributed deformation and apparent high elastic loading in Sumatra are opposed to apparently localized deformation in Java. This corroborates records of the last 200 years that indicate that Sumatra has been struck by several large to major earthquakes (Newcomb & McCann 1987) whereas the margin along Java has been—except for a large earthquake on June 2 1994 (e.g. CMT Harvard catalogue; Dziewonski *et al.* 1981)—seismically almost quiet.

Regional seismic moments derived by Pacheco & Sykes 1992) for the time span between 1900 and 1989 suggest significantly higher cumulative moment rates than derived in this study for both the Manila (MANN, MANS, Fig. 6) and the Cotabato (COTO, Fig. 6) subduction segments. In view of the geodetically derived rates, this suggests that the Cotabato fault has not accumulated large strains to date, whereas localized deformation and an incapacity for strain accumulation along the Manila trench is questionable at least for a time span larger than that considered in this study. This might indicate that (i) the NUVEL1A solution for the Philippine Sea plate is not accurate, (ii) additional extension along the Manila fore-arc, for example, due to subduction roll-back, obliterates surface straining, and/or (iii) the results of the last few years of measurements along this arc do not have long-term validity.

The penultimate devastating earthquakes to the southeast of Sumatra occurred in 1914 ($M_s=7.6$) and 1908 ($M_s=7.6$) (Newcomb & McCann 1987). The last earthquake that apparently ruptured the entire segment (Fig. 6, SU2T) occurred in 1833 ($M_s\sim8.7$). This suggests that strain accumulation in southeast Sumatra may be extrapolated over 90 years. Full coupling during this time span would, however, result in a one-half–one order of magnitude higher accumulated moment (4×10^{21} N m) along this part of the margin than was released by the 2000 June 4 earthquake (7.3×10^{20} N m). Our results indicate that the rupture process for this earthquake was complex, suggesting that motion occurred along a compound fault. The mechanism of the largest subevent of the best-fitting

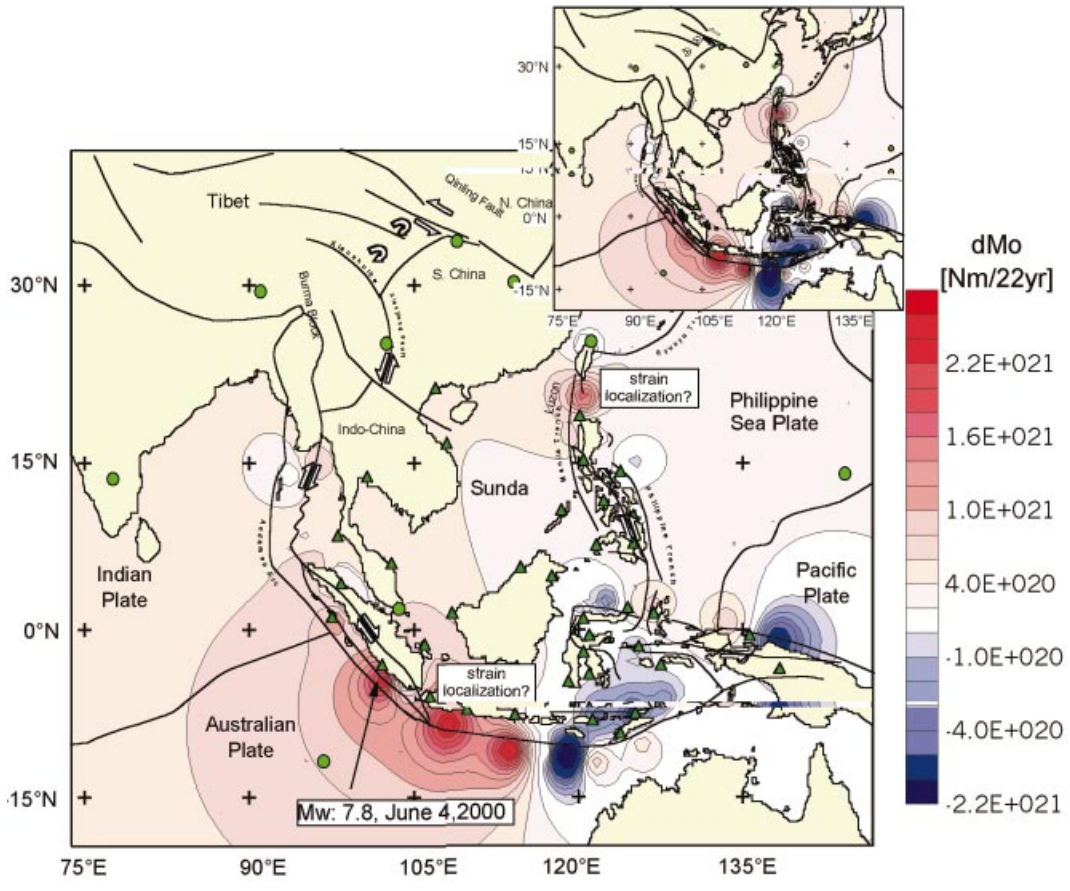

Figure 7. Total implied moment (accumulated geodetic versus seismic deformation, 'moment budget') from January 1977 to June 1999. Taking into account that GPS data suggest localized deformation and hence apparent creep along both the Manila trench and the Java margin, the largest accumulated deformation derived is located where the 2000 June 4 earthquake occurred near southeast Sumatra. Dots denote permanent stations (IGS 1998) and triangles depict GEODYSSEA GPS sites. The large figure depicts results from computations that include fault segment dimensions as defined in Table 1; fault segment lengths were averaged in order to derived the 'moment budget' in the upper right of the figure (see text for discussion).

model approximates the cumulative mechanism inferred by the historical interplate earthquakes (Figs 3 and 8), whereas the two smaller events display slip along fault planes rotated by $\sim 30^{\circ}$. This suggests that the accommodation of deformation to the southeast of Sumatra is complex. This might reflect the beginning of a change in deformational behaviour within the Sunda arc between Sumatra and Java and a highly fractured plate interface further to the east along the Sunda arc. The variable directions in faulting, as indicated by the inversion method, may represent a mesh of faults that may not be able to accumulate high stresses, and deformation may be localized, as suggested above. An additional explanation for the complex coseismic fault pattern derived may be local fracturing of the Sumatran fore-arc sliver at its southeastern termination, where it is assumed to suffer subsequent cycles of thrusting and strike-slip faulting.

One critical aspect of approximating geodetic and seismic moment rates as applied here lies in the definition of fault segment dimensions. Owing to the different levels of information collected from different literature sources, the regional geology and seismotectonic approaches, the relative segment lengths in particular appear to be questionable. In order to check the influence of the segment lengths on the total implied moment, a uniform-length solution was approximated (Fig. 7). The results of this model do not change the ratio between geodetic and seismic moment rates. If the moments are highly dependent on the segment dimensions rather than the slip rates, this solution would account for a different distribution in 'moment budget'. The results, however, approximate a solution essentially similar to the solution of the more complex model with segment dimensions as shown in Fig. 3 or Table 1. Considering that the differences in depth range of the segments investigated are small compared to the differences in moments, we conclude that the solution is (relatively) robust with respect to errors in fault dimensions.

Overall rates of seismic versus geodetic deformation reveal a ratio of 0.7 for the area under study and the studied time span. This suggests that a considerable portion of the margins investigated undergoes high seismogenic coupling. Although high plate convergence rates of up to 80 mm yr^{-1} suggest that recurrences intervals of large earthquakes may be small and may reach the time span studied, larger intervals are expected for most of the plate and block margins considered here. Further studies are therefore needed to investigate incremental rates of earthquake occurrence as a function of magnitude (see e.g. Field *et al.* 1999) and/or historical and palaeoseismological records from the area in detail. Static and dynamic redistribution of strains and stresses during or after earthquakes, including post-seismic time-dependent relaxation of the lower crust and upper mantle, may change the overall picture to some extent

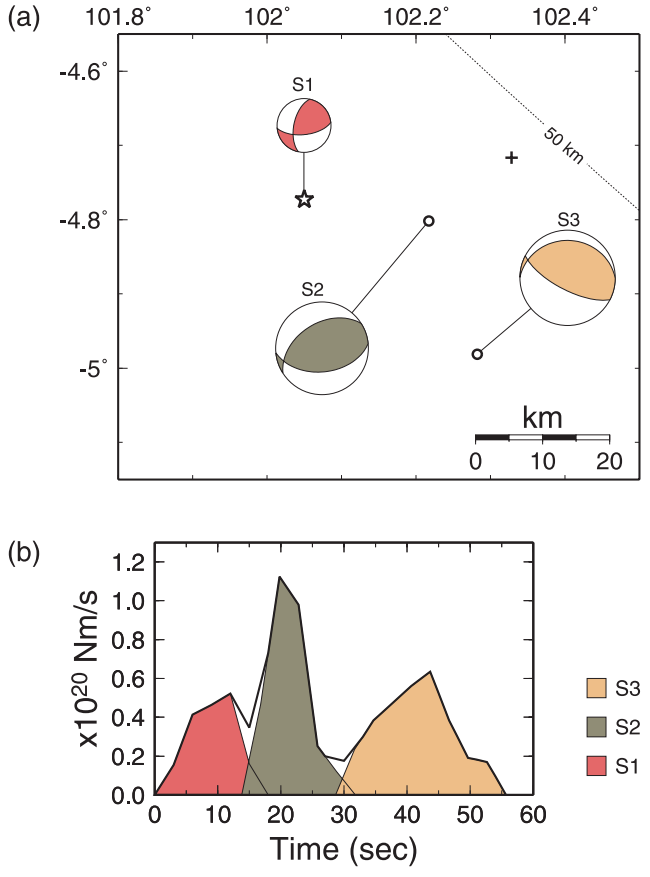

Figure 8. (a) Map showing the locations of the subevents S1, S2 and S3 of the preferred source model of the 2000 June 4 Sumatra earthquake. The plus sign in the figure denotes the centroid location. The dashed line represents the 50 km depth contour line of the seismogenic zone (Gudmundsson & Sambridge 1998). (b) The source time function for the three subevents, and the whole rupture process (thick line).

and may indicate higher or lower accumulated moments in the vicinity of large earthquakes. A detailed study of this subject has already been launched for the area.

6 CONCLUSIONS

The results from our geodetic and seismotectonic study in Southeast Asia helped to constrain slip and moment rates and a regional kinematic fault-and-block model for the area. Assuming that geodetic rates approximate seismic loading rates, and comparing these rates with the moment rates implied by the seismicity over the time span between 1977 and 2000, the results suggest that a large portion of the measured deformation has been accommodated by seismic deformation. Apparent discrepancies along the eastern Sunda arc and along the Manila arc from a full seismogenic coupling model describing apparent elastic deformation along the major faults in the area were detected. This suggests that elastic loading varies spatially and/or temporally along the investigated plate margins. Assuming that the deformation conditions derived are representative of longer time spans, and lower ratios in seismogenic faulting versus geodetic deformation reflect higher probabilities of large future earthquakes, we suspect that the southeastern Sumatra margin, the western North Guinea trench and the Halmahera–Sanghie region represent locations where large earthquakes are more likely to occur in the future than elsewhere in the region. Additionally, at least the Java and Manila margins need to be monitored further in order to gain a better understanding of transient effects related to apparently localized deformation there. The 2000 June 4, $M_w = 7.8$, Sumatra earthquake that occurred after the time span covered by the data used here falls into the region of the highest deficit in seismogenic faulting discussed in this study. We therefore conclude that the straightforward 'moment budget' approach may offer possibilities for future applications if geodetic information on the loading conditions is discussed.

REFERENCES

Becker, M., Reinhart, E., Bin Nordin, S., Angermann, D., Michel, G.W. & Reigber, Ch., 2000. Improving the velocity field in South and South-East Asia: the third round of GEODYSSEA, *Earth Planets Space,* **52,** 721–726.

Cardwell, R.K., Isacks, B.L. & Karig, D.E., 1980. The spatial distribution of earthquakes, focal mechanism solutions and subducted lithospheres in the Philippines and Northern Indonesian region, in *The Tectonic and Geologic Evolution of South-East Asian Seas and Islands,* ed. Hayes, D.E., *Geophys. Un. Monogr.,* **23,** 1–35.

Chamot-Rooke, N. & Le Pichon, X., 1999. GPS determined eastward Sundaland motion with respect to Eurasia confirmed by earthquakes slip vectors at Sunda and Philippine trenches, *Earth planet. Sci. Lett.,* **173,** 439–455.

Chen, Z. *et al.*, 2000. Global Positioning System measurements from Eastern Tibet and their implications for India/Eurasia intercontinental deformation, *J. geophys. Res.,* **105,** 16 215–16 227.

DeMets, C., Gordon, R.G., Argus, D.F. & Stein, S., 1990. Current plate motion, *Geophys. Res. Lett.,* **101,** 425–478.

DeMets, C., Gordon, R.G., Argus, D.F. & Stein, S., 1994. Effects of recent revisions to the geomagnetic reversal time scale on estimates of current plate motions, *Geophys. Res. Lett.,* **21,** 2191–2194.

Duquesnoy, T. *et al.*, 1994. Detection of creep along the Philippine Fault: first results of geodetic measurements on Leyte island, central Philippine, *Geophys Res. Lett.,* **21,** 975–978.

Dziewonski, A.M., Chou, T.-A. & Woodhouse, J.H., 1981. Determination of earthquakes source parameters from waveform data for studies of global and regional seismicity, *J. geophys. Res.,* **86,** 2825–2852.

Field, E.H., Jackson, D.D. & Dolan, J.F., 1999. A mutually consistent seismic-hazard source model for Southern California, *Bull. seism. Soc. Am.,* **89,** 559–578.

Freymueller, J.T. & Beaven, J., 1999. Absence of strain accumulation in the western Shumagin segment of the Alaska subduction zone, *Geophys Res. Lett.,* **26,** 3233–3236.

Genrich, J. *et al.*, 1996. Accretion of the southern Banda arc to the Australian plate margin determined by Global Positioning System measurements, *Tectonics,* **15,** 288–295.

Gordon, R.G., DeMets, C. & Argus, D.F., 1990. Kinematic constraints on distributed lithospheric deformation in the equatorial Indian Ocean from present motion between the Australian and Indian plates, *Tectonics,* **9,** 409–422.

Gordon, R.G., DeMets, C. & Royer, J.Y., 1998. Evidence for long-term diffuse deformation of the lithosphere of the equatorial Indian Ocean, *Nature,* **24,** 370–374.

Gudmundsson, O. & Sambridge, M., 1998. A regionalized upper mantle (RUM) seismic model, *J. geophys. Res.,* **103,** 7121–7136.

Hamilton, W., 1979. Tectonics of the Indonesian region, *USGS Paper,* **1078,** 1–345.

IGS, International GPS Service for Geodynamics, 1998. *IGS Electronic Mail*, Message no. 2071, IGS Central Bureau, Jet Propulsion Laboratory, California Institute of Technology, Pasadena, CA.

Kennett, B.L.N. & Engdahl, E.R., 1991. Taveltimes for global earthquake location and phase identification, *Geophys. J. Int.,* **105,** 429–465.

Kostrov, V.V., 1974. Seismic moment and energy of earthquakes and the seismic flow of rock, *Izvestiya, Akademi Naul, USSR, Phys. Solid Earth,* **1,** 23–44 (in Russian).

Kreemer, C., Holt, W.E., Goes, S. & Govers, R., 2000. Active deformation in eastern Indonesia and the Philippines from GPS and seismicity data, *J. geophys. Res.,* **105,** 663–680.

McCaffrey, R., 1996. Slip partitioning at convergent plate boundaries of SE Asia, in *Tectonic Evolution of South-east Asia,* eds Hall, R. & Blundell, D. J., *Geol. Soc. Spec. Publ.,* **106,** 3–18.

Michel, G.W., Becker, M., Angermann, D., Reigber, Ch. & Reinhart, E., 2000. Crustal motion in E and SE Asia from GPS measurements, *Earth Planets Space,* **52,** 713–720.

Nábelek, J.L., 1984. Determination of earthquake source parameters from inversion of body waves, *PhD thesis,* MIT, Cambridge, MA.

Newcomb, K.R. & McCann, W.R., 1987. Seismic history of the Sunda Arc, *J. geophys. Res.,* **92,** 421–439.

Okada, Y., 1985. Surface deformation due to shear and tensile faults in a half-space, *Bull. seism. Soc., Am.,* **75,** 1135–1154.

Pacheco, J.F. & Sykes, L.R., 1992. Seismic moment catalogue of large shallow earthquakes, 1900–1989, *Bull. seism. Soc., Am.,* **82,** 1306–1349.

Peltzer, G. & Saucier, F., 1996. Present-day kinematics of Asia derived from geologic fault rates, *J. geophys. Res.,* **101,** 27 943–27 956.

Pollitz, F. & Dixon, T.H., 1998. GPS measurements across the northern Caribbean plate boundary zone: impact of postseismic relaxation following historic earthquakes, *Geophys. Res. Lett.,* **25,** 2233–2236.

Prawirodirdjo, L. *et al.*, 1997. Geodetic observation of interseismic strain segmentation at the Sumatra subduction zone, *Geophys. Res. Lett.,* **24,** 2601–2604.

Puntodewo, S.S. *et al.*, 1994. GPS measurements of crustal deformation within the Pacific–Australia plate boundary zone in Irian Jaya, Indonesia, *Tectonophysics,* **237,** 141–153.

Rangin, C.X., Le Pichon, X., Mazzotti, S., Pubellier, M., Chamot-Rooke, N., Aurelio, M., Walpersdorf, A. & Quebral, R., 1999. Plate convergence measured by GPS across the Sundaland/Philippine Sea Plate deformation boundary: Philippines and eastern Indonesia, *Geophys. J. Int.,* **139,** 296–316.

Savage, J.C.A., 1983. Dislocation model of strain accumulation and release at a subduction zone, *J. geophys. Res.,* **88,** 4988–4996.

Scholz, C.H., 1982. Scaling laws for large earthquakes, consequences for physical models, *Bull. seism. Soc. Am.,* **82,** 1–14.

Scholz, C.H. & Aviles, C., 1986. The fractal geometry of faults and faulting, in *Earthquake Source Mechanisms,* eds Das. S, Boatwright, J. & Scholz, C., *AGU Geophys. Monogr.,* **37,** 147–155.

Simons, W.J.F. *et al.*, 1999. Plate motions in South-East Asia: results of the GEODYSSEA project, *Geophys. Res. Lett.,* **26,** 2081–2084.

Stein, R.S., Barka, A.A. & Dietrich, J.H., 1997. Progressive failure of the North Anatolian Fault since 1939 by earthquake stress triggering, *Geophys. J. Int.,* **128,** 594–604.

Tjia, H.D., 1978. Active faults in Indonesia, *Geol. Soc. Malaysia,* **10,** 73–92.

Tregoning, P. *et al.*, 1994. First geodetic measurements of convergence across the Java Trench, *Geophys Res. Lett.,* **21,** 2135–2138.

Wells, D.L. & Coppersmith, K.J., 1994. New empirical relationships among magnitude, rupture length, rupture width, rupture area and surface displacement, *Bull. seism. Soc. Am.,* **84,** 974–1002.

Wilson, P. *et al.*, 1998. The GEODYSSEA project: an investigation of the geology and geodynamics of South and South-East Asia, *EOS, Trans. Am. geophys. Un.,* **79,** 548–549.

Yu, S.B. & Liu, C.C., 1989. Fault creep on the central segment of the Longitudinal Fault, eastern Taiwan, *Proc. Geol. Soc. China,* **32,** 209–231.

Yu, S.-B., Kuo, L.-C., Punongbayan, S. & Ramos, E.G., 1999. GPS observation of crustal deformation in the Taiwan, Luzon region, *Geophys. Res. Lett.,* **26,** 923–926.